Biosensors and Bioelectronics 142 (2019) 111521

Contents lists available at ScienceDirect

Biosensors and Bioelectronics

journal homepage: www.elsevier.com/locate/bios

Double electrochemiluminescence quenching effects of Fe_3O_4@PDA-Cu_XO towards self-enhanced Ru(bpy)$_3^{2+}$ functionalized MOFs with hollow structure and it application to procalcitonin immunosensing

Chao Wang[a], Nuo Zhang[a], Dong Wei[b], Rui Feng[b], Dawei Fan[a], Lihua Hu[a,**], Qin Wei[a,*], Huangxian Ju[a]

[a] Key Laboratory of Interfacial Reaction & Sensing Analysis in Universities of Shandong, School of Chemistry and Chemical Engineering, University of Jinan, Jinan, 250022, China

[b] School of Water Conservancy and Environment, University of Jinan, Jinan, 250022, China

ARTICLE INFO

Keywords:
Electrochemiluminescence
Self-enhanced
Ru(bpy)$_3^{2+}$
Mesoporous MOF
Double quenching
Polydopamine
Procalcitonin

ABSTRACT

The rapid and reliable measurement of procalcitonin (PCT) level exerts a prominent impact on controlling infections and preventing septicemia. This work presents a "signal on-off" electrochemiluminescence (ECL) immunosensor for ultrasensitive PCT detection based on the double quenching effects of Fe_3O_4@PDA-Cu_xO towards a self-enhanced Ru (bpy)$_3^{2+}$-functionalized metal organic framework (MOF). Specifically, mesoporous and hollow MIL-101(Al)–NH_2 is first applied in ECL system to load Ru (bpy)$_3^{2+}$ abundantly and stably. Poly (ethylenimine), as the coreactant, is covalently linked with MIL-101(Al)–NH_2 to prevent the leakage of Ru (bpy)$_3^{2+}$ and form a self-enhanced Ru complex, thus strong and stable ECL signals are obtained initially. To achieve high-efficiency quenching of "signal on" state, Fe_3O_4@PDA-Cu_xO-Ab_2 is synthesized tactfully as the quenching probe by which catechol or benzoquinone units in PDA and Cu^{2+} adsorbed by PDA quench the excited states of Ru (bpy)$_3^{2+}$ via electron transfer and resonance energy transfer. In this way, a rapid and robust signal-quenched type ECL immunosensor is developed for PCT measurement with a detection limit of 0.18 pg mL^{-1} and a dynamic range from 0.0005 ng mL^{-1} to 100 ng mL^{-1}. Given desirable selectivity, stability and reproducibility, the elaborated ECL immunoassay based on luminescence-functionalized MOF prefigures its great promise in bioanalysis of PCT and other biomarkers.

1. Introduction

Septicemia, a life-threatening health problem globally, is recognized as a kind of systemic inflammatory response caused by infections, particularly for bacterial infections (Zhang et al., 2018). Patients who suffer from cancer and bear chemotherapy are at great risk to develop infections and even worsen to septicemia (El Haddad et al., 2018). Without treatment in time, septicemia can rapidly result in organ dysfunction, tissue damage and death. Therefore, the accurate and timely diagnosis of septicemia is of crucial significance and clinical necessity. Procalcitonin (PCT), a 116-amino-acid protein with a molecular mass of 13 kDA, has been explored as a reliable prognostic and therapeutic indicator of septicemia (Vincenzi et al., 2016). The PCT level in serum of healthy individual is below 0.1 ng mL^{-1}, while it advances to over several-thousand-fold with the severity of infections and septicemia (Li et al., 2018). Thus far, despite a variety of analytical approaches (e.g. electrochemical (Fang et al., 2018), surface plasma resonance (Sener et al., 2013) and optical (Baldini et al., 2009)) have been applied to measure PCT concentrations, these methods still remain some challenges in operational convenience and sensitivity. Against this backdrop, electrochemiluminescence (ECL), as the marriage of electrochemistry and chemiluminescence, has become a burgeoning and powerful analytical technique in virtue of low background noise, simplified optical equipment and high sensitivity (Hao et al., 2013; Li et al., 2017a). However, applying ECL technique in quantification of PCT has rarely been reported till now. Herein, developing a highly sensitive ECL immunosensor for PCT detection is in great demand.

With the goal of improving sensitivity of ECL immunosensors, numerous analytical tactics including ratio-dependent type (Wang et al., 2016b), signal-enhanced type (Wang et al., 2016a) and signal-quenched

* Corresponding author.
** Corresponding author.
E-mail addresses: hulihua1206@163.com (L. Hu), sdjndxwq@163.com (Q. Wei).

https://doi.org/10.1016/j.bios.2019.111521
Received 22 May 2019; Received in revised form 11 July 2019; Accepted 15 July 2019
Available online 19 July 2019
0956-5663/

type (Yang et al., 2013) ECL immunoassay have been proposed. Signal-quenched type, also known as "signal on-off", has captured great research attention in the realm of ECL owing to its low detection limit and rapid response. The precondition to achieve high sensitivity in "signal on-off" ECL system is that the initial ECL signal must be strong and stable, while it is predominately concerned with effective signal amplification strategy. Since the exploration of electrochemiluminophore tris(2, 2′-bipyridyl) ruthenium (II) (Ru $(bpy)_3^{2+}$) in 1972 (Tokel and Bard, 1972), Ru $(bpy)_3^{2+}$ and its derivatives have become the most extensively investigated ECL materials in view of their long excited-state lifetime, reversible electrochemical behavior, broad application range for pH and high luminescence efficiency. Nonetheless, due to the fine solubility of Ru $(bpy)_3^{2+}$ in water, it is still a tough nut to seek efficient methods for immobilizing Ru $(bpy)_3^{2+}$ on the electrode surface. Given the high surface area, versatile tunability of pore size as well as intrinstic electronic and dimensional structure diversity, metal organic frameworks (MOFs) are foreseen as promising candidates for application in biosensing field (Zhu and Xu, 2014). In particular, luminescence-functionalized MOFs, which integrate the electrochemiluminophore into the skeleton or cavity of MOFs, afford a novel platform to maximum the loading capacity of luminophore (Cui et al., 2012; Qin et al., 2018). Synthesized by using 2-aminoterephthalic acid (BDC-NH_2) as the ligand and Al^{3+} as the metal cluster, the MIL-101(Al)–NH_2 (where MIL represents Materials of Institute Lavoisier) is built up from super-tetrahedral building units which possesses two kinds of spherical mesoporous cavities with diameters of 1.2 nm and 1.6 nm, respectively (Haque et al., 2014). Such excellent pore size distribution is beneficial to encapsulate Ru $(bpy)_3^{2+}$ into the interior of MIL-101(Al)–NH_2 since the size of Ru $(bpy)_3^{2+}$ is within 1.2 nm. Hence, by elaborately adjusting the precursor ratio and reaction condition, an innovative luminescence-functionalized MOF denoted as MIL-101(Al):Ru was prepared in this work which possesses large surface area and intrinstic mesoporous structure to load Ru $(bpy)_3^{2+}$ abundantly in a stable immobilization routing.

Since Yuan's group proposed the signal amplification strategy of "self-enhanced ECL complex" in 2013 (Zhuo et al., 2014), a wealth of literatures has provided invaluable enlightment for designing self-enhanced ECL sensors with high luminous efficiency and sensitivity. By covalently coupling the luminophore with appropriate coreactant in one nanostructure, self-enhanced ECL composites could not only simplify operation process and save analytical time, but also diminish the electron transmission path and reduce energy loss (Zhou et al., 2018). For that reason, a remarkable breakthrough has been made in exploiting effective coreactants of Ru $(bpy)_3^{2+}$, such as poly-L-lysine (Liao et al., 2013), dendrimer PAMAM (Wang et al., 2015) and so forth. Among these coreactants, as an amine-rich polymer, poly (ethylenimine) (PEI) is of ongoing interest in binary system of luminophore and coreactant (Liao et al., 2012). Inspired by these discussions, a self-enhanced Ru-PEI complex which combined Ru $(bpy)_3^{2+}$ functionalized MOF with PEI of many coreactive tertiary amidogen was synthesized in this work (abbreviated as MIL-101(Al):Ru-PEI) to acquire stable and strong ECL initial signals. More notably, the leakage of Ru $(bpy)_3^{2+}$ from MIL-101(Al)–NH_2 was inhibited tactfully with PEI wrapped on the surface of MOF. Meanwhile, considering the poor conductivity of MIL-101(Al)–NH_2, Au NPs were immobilized on the MIL-101(Al):Ru-PEI via Au–NH_2 bond to improve the electron transfer ability.

Quench efficiency is reckoned as another crucial point for "signal on-off" system. Apart from the commonly used quenchers such as hemin (Hong et al., 2015), ferrocene (Lei et al., 2016) and carbon-based nanomaterials (Li et al., 2017b), past efforts have indicated that dopamine and polydopamine (PDA) with catechol or benzoquinone units in their structure could be employed as effective quenching probes for ECL system (Wang et al., 2017; Zhao et al., 2016). Since an innovative report about PDA was appeared in 2007 (Lee et al., 2007), PDA has been extensively applied in biosensing and biomedicine fields for its appealing features of excellent biocompatibility, strong adhesive ability and easy of functionalization (Hu et al., 2014). By selecting Fe_3O_4 nanoparticles as the biomolecule carriers, dopamine could form thin PDA shell on the surface of Fe_3O_4 via self-polymerization process, endowing the resulted core-shell polymer material with magnetically susceptible characteristics. Moreover, PDA could react with amines and thiols of protein via Schiff base reaction or Michael addition reaction, thereafter antibodies are able to attach on the surface of PDA directly without employing any activation procedure, making it a versatile platform for immunosensing. It is worth highlighting that PDA could purify waste water from heavy metal ions containing Cu^{2+} through adsorption (Zhang et al., 2014), whereas it has been reported that Cu^{2+} could inhibit the emission of luminophore due to excited-state energy transfer or electron transfer (Mei et al., 2010; Yue et al., 2015). Taking the advantage of adsorption ability of PDA towards Cu^{2+}, an effective quenching probe (Fe_3O_4@PDA-Cu_xO-Ab_2) with double quenching effects of PDA and Cu^{2+} was prepared, which led to a prominent inhibition of the initial ECL signal. Compared with the UV–vis spectra of Fe_3O_4@PDA, a broader absorption range was acquired from Fe_3O_4@PDA-Cu_xO, enabling the noticeable overlap with the ECL emission spectra of MIL-101(Al):Ru, thus the occurrence of resonance energy transfer (RET) between the energy donor of Ru@MIL-101 and the energy acceptor of Fe_3O_4@PDA-Cu_xO was triggered. In this way, an elaborated ECL "signal on-off" protocol based on the double quenching effects of Fe_3O_4@PDA-Cu_xO towards self-enhanced MIL-101(Al):Ru-PEI-Au was proposed in this work for ultrasensitive determination of PCT. This immunosensor exhibited desirable linear response to PCT concentration varied from 0.0005 ng mL^{-1} to 100 ng mL^{-1}, which not only pioneered an alternative strategy for preparing luminescence-functionalized MOFs, but also prefigured its great promise in accurate measurement of PCT and other biomarkers.

2. Experimental section

2.1. Construction of ECL immunosensor

Prior to modification, glassy carbon electrode (GCE, 4 mm in diameter) was pretreated by 0.05 μm alumina slurry and washed with ultrapure water to get a smooth and clear surface. Then, 6 μL of MIL-101(Al):Ru-PEI-Au was casted onto the electrode and dried at normal temperature (20 °C). Subsequently, 5 μL of Ab_1 (10 μg mL^{-1}) was assembled on the electrode via Au–NH_2 bond. Later, the immunosensing interface was rinsed cautiously by PBS (pH 7.4) and modified with 3 μL of BSA (1 wt%) to block the possible nonspecific binding sites. Followed that, 6 μL of PCT antigen with different concentrations (varied from 0.0005 ng mL^{-1} to 100 ng mL^{-1}) was decorated on the electrode and incubated at 4 °C overnight. Eventually, the electrode was washed with PBS (pH 7.4) to remove the non-specifically bonded antigens and immobilized with 6 μL of Ab_2 bioconjugates. After the immune-complexes were formed, the unreacted Ab_2 were washed away by PBS (pH 7.4). The fabrication process was shown in Scheme 1.

2.2. ECL detection of PCT

ECL detection were conducted by a MPI-F 193 flow-injection chemiluminescence detector (Xi'an Remax Electronic Science Tech. Co. Ltd., China) in 10 mL of PBS (pH 7.4) under the potential scan from 0 V to 1.2 V. The voltage of photomultiplier tube and the scan rate were set at 600 V and 100 mV s^{-1}, respectively. With the increment of PCT concentration, more Ab_2 bioconjugates were immobilized on the electrode, which led to stronger inhibition of ECL signals. Based on the changes of ECL response, the concentration of PCT antigens could be measured quantitatively.

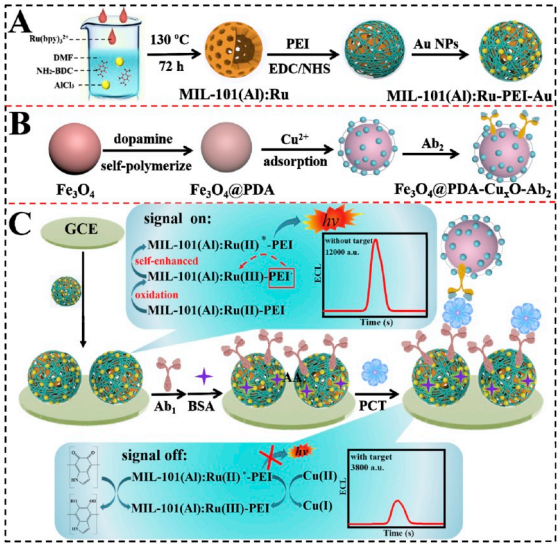

Scheme. 1. Schematic diagrams for (A) the synthesis steps of MIL-101(Al):Ru-PEI-Au, (B) the synthesis steps of Fe_3O_4@PDA-Cu_xO-Ab_2, (C) the fabrication process of PCT sensor and the possible luminescence mechanism.

3. Results and discussion

3.1. Characteristics of different nanomaterials

Scanning electron microscopy (SEM) and transmission electron microscopy (TEM) were employed to characterize the morphology and structure of these nanomaterials. As demonstrated in Fig. 1A, the MIL-101(Al):Ru presented a uniform spherical nanostructure with tiny salient points on its surface, and the average diameter was 550 ± 50 nm. Fig. 1B displayed the SEM image of broken MIL-101(Al):Ru nanosphere, which indicated preliminarily that MIL-101(Al):Ru was of hollow structure with the thickness of shell around 150 nm. The TEM image of MIL-101(Al):Ru with bright pattern in its center, which was exhibited in the inset of Fig. 1B, further confirmed the hollow and porous structure of the luminescence functionalized MOF. Fig. 1C was the TEM image of MIL-101(Al):Ru-PEI-Au, from which substantial Au NPs were observed clearly on the surface of MIL-101(Al):Ru-PEI. In the inset of Fig. 1C, the high resolution TEM image of Au NPs exhibited sphere morphology with a mean diameter of 12 nm. The typical SEM image of Fe_3O_4 (Fig. 1D) revealed a well-defined sphere shape with diameter of 200 nm. As clearly observed from Fig. 1E, a thin polydopamine shell of approximately 10 nm in thickness was wrapped uniformly on the rough surface of Fe_3O_4 nanoparticle. From the high magnification TEM image (Fig. 1F), it was obvious that the adsorption of copper ion by PDA layers made little influence on the morphology of Fe_3O_4@PDA. The inset of Fig. 1F was the energy dispersive spectrometer (EDS) result of Fe_3O_4@PDA-Cu_xO, from which we could find that the quenching probe was made up of Fe, Cu, C, N and O elements.

TEM mapping images with distinct color contrast for elements Fe, Cu, C, N and O were illustrated in Fig. 2A. The high overlap and uniform distribution of these elements further proved the successful preparation of Fe_3O_4@PDA-Cu_xO nanoparticles. Moreover, X-ray diffraction (XRD) of Fe_3O_4@PDA-Cu_xO was also conducted and the results were presented in Fig. 2B. All the characteristic diffraction peaks could be matched well with the face centered cubic of Fe_3O_4 (JCPDS card No. 19–0629). On account of the amorphous crystalline property of PDA, the PDA coating did not alter the crystalline phase of pristine Fe_3O_4. It was noteworthy that the highest diffraction peak located at around 35.5°, as we can see from the inset of Fig. 2B, was derived from (002) plane of CuO (JCPDS card No. 02–1040) and (311) plane of Fe_3O_4, which verified the success of Fe_3O_4@PDA-Cu_xO synthesis. The XRD pattern of MIL-101(Al):Ru (Fig. 2C) was similar to that of simulated MIL-101 (Cr) and no diffraction peak of Ru $(bpy)_3^{2+}$ was observed, manifesting that Ru $(bpy)_3^{2+}$ has been embedded in the interior of MIL-101. Furthermore, the infrared spectra of NH_2-BDC and MIL-101(Al):Ru were also investigated to prove the existence of carboxyl group in MIL-101(Al):Ru. As shown in Fig. 2D, the broad peak displayed in region of 3100–2800 cm^{-1} was assigned to the O–H stretching vibration, and the wavenumber located at 1670 cm^{-1} arose from C=O stretching vibration in –COOH. The peaks located at 1440 cm^{-1} and 1260 cm^{-1} were O–H in-plane bending vibration, which were overlapped with C–O stretching vibration. The characteristic absorption of O–Al stretching vibration appeared at 590 cm^{-1} validated the coordination of –COOH to Al^{3+}. The above discussions certified the existence of carboxyl group in MIL-101(Al):Ru, thus PEI could covalently linked with MIL-101(Al):Ru to form a self-enhanced nanostructure.

For more precisely exploring the chemical composition and valence state of as-synthesized materials, X-ray photoelectron spectroscopic (XPS) analysis was provided in Fig. S1. In Fig. S1A, the XPS survey

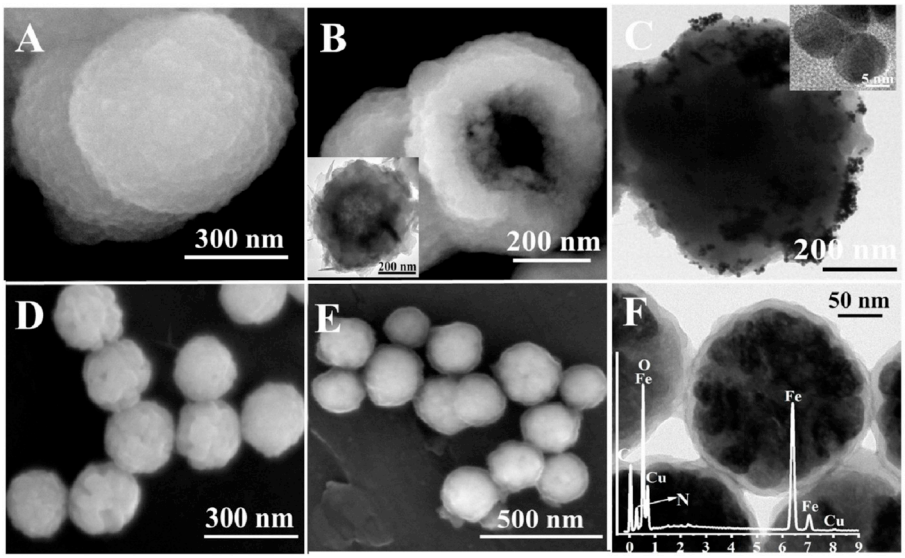

Fig. 1. (A) (B) SEM image of MIL-101(Al):Ru. (C) TEM image of MIL-101(Al):Ru-PEI-Au. The inset of (B) and (C): TEM image of MIL-101(Al):Ru and Au NPs. (D) SEM image of Fe_3O_4. (E) SEM image of Fe_3O_4@PDA. (F) TEM image of Fe_3O_4@PDA-Cu_xO. The inset of (F): EDS result of Fe_3O_4@PDA-Cu_xO.

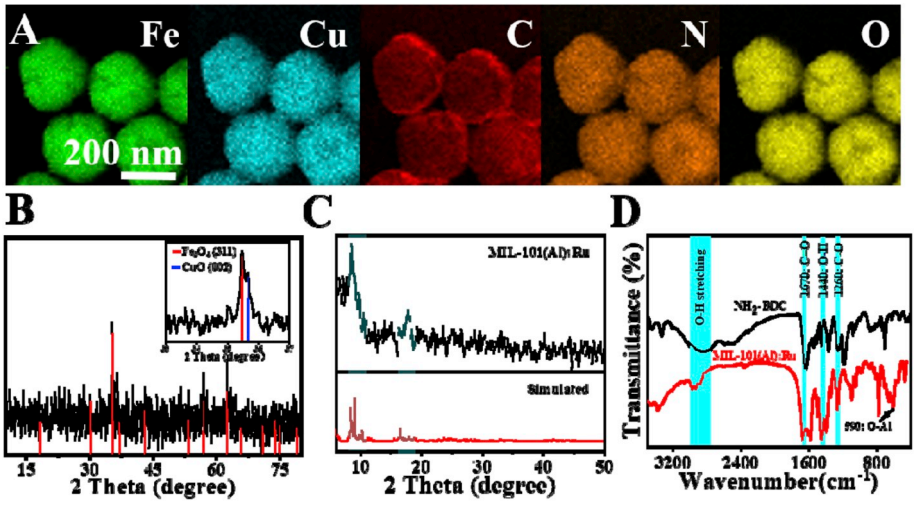

Fig. 2. (A) TEM mapping images of Fe, O, Cu, C, N elements in Fe_3O_4@PDA-Cu_xO. (B) XRD pattern of Fe_3O_4@PDA-Cu_xO. (C) XRD pattern of MIL-101(Al):Ru. (D) Infrared spectra of NH_2-BDC and MIL-101(Al):Ru.

spectra of Fe_3O_4@PDA-Cu_xO demonstrated the presence of Cu, Fe, C, N and O elements in the sample. The Cu 2p region exhibited two main peaks with binding energies (BEs) at 933 and 953 eV, which were corresponded to Cu $2p^{3/2}$ and Cu $2p^{1/2}$, respectively. The fitting peaks located at 934.5 and 954.3 eV for Cu^{2+} species, 932.7 and 952.0 eV for Cu^{+} species as well as the satellite peaks (defined as "sat.") at 944.0 eV for Cu^{2+} and 942.0 eV for Cu^{+} suggested that the surface copper ions were existed in two valence states. The larger peak area of Cu^{2+} implied that Cu^{2+} was the majority of copper ion. Meanwhile, the BE at 571.0 eV in the Cu LM2 Auger spectra, which was ascribed to Cu^{+}, further confirmed the existence of Cu^{+} on the surface of Fe_3O_4@PDA. The above analysis manifested that copper ions were adsorbed by the PDA shell and formed Cu_2O and CuO, thus the quenching probe was named as Fe_3O_4@PDA-Cu_xO.The BEs of C 1s region appeared at 284.6, 285.9 and 288.3 eV, which were assigned to C═C/C–C, C═N/C–O and C═O, respectively, indicating the well-coated PDA shell on Fe_3O_4 nanoparticles. Additionally, as shown in Fig. S1B, the peaks at around 532, 400, 285 eV in the survey spectra of MIL-101(Al):Ru were well matched to O 1s, N 1s and C 1s, respectively. Moreover, the high-resolution XPS spectra of Ru 3p, Au 4f and Al 2p demonstrated the presence of Ru, Au and Al elements in MIL-101(Al):Ru. The above XPS results further proved the successful preparation of these biosensing materials.

3.2. ECL mechanism of MIL-101(Al):Ru-PEI-Au and quenching mechanism of Fe_3O_4@PDA-Cu_xO

Control experiments were carried out to illustrate the superiority of MIL-101(Al):Ru-PEI-Au and the ECL signal amplification tactics. As displayed in Fig. 3A, the ECL signal of MIL-101(Al):Ru-PEI-Au modified electrode (curve a) was approximately 3000 a. u. stronger than that of MIL-101(Al):Ru-PEI modified electrode (curve b), demonstrating that Au NPs could enhance the ECL emission of Ru $(bpy)_3^{2+}$ (Du et al., 2018). Meanwhile, we also investigated the role of PEI played in the ECL of MIL-101(Al):Ru by detecting ECL responses of MIL-101(Al):Ru modified electrodes in different working buffers. The ECL response of MIL-101(Al):Ru modified electrode with tripropylamine (TPrA) as the coreactant (curve c) was merely half of that with PEI as the coreactant (curve d), thus PEI was chosen as the coreactant of MIL-101(Al):Ru. Furthermore, as is clearly shown in Fig. 3B, whether the coreactant PEI was covalently bound with the luminescence functionalized MOF or dropped into the working buffer made a pronounced difference in the ECL emission of MIL-101(Al):Ru. The MIL-101(Al):Ru-PEI self-enhanced ECL complex (curve a) presented a higher ECL response (ΔI = 4224 a. u.) than that of MIL-101(Al):Ru with PEI dropped in the electrolyte (curve b). Additionally, the time it took to achieve the maximum ECL signal was faster for the self-enhanced Ru complex, manifesting that MIL-101(Al):Ru-PEI composites could effectively lower the energy loss and enhance ECL efficiency of Ru $(bpy)_3^{2+}$ due to the short transmission distance of energy and charge offered by intramolecular reaction. The possible ECL mechanisms of MIL-101(Al):Ru-PEI were outlined as follows according to previous literature (Chen et al., 2017; Xiong et al., 2017; Zhao et al., 2015). In such a ECL mechanism, the luminous species, MIL-101(Al):Ru (II)*, was produced by the intramolecular electron transport between PEI· and Ru (III).

$$MIL-101(Al):Ru(II)-PEI-2e^{-} \rightarrow MIL-101(Al):Ru(III)-PEI^{+} \quad (1)$$

$$MIL-101(Al):Ru(III)-PEI^{\cdot +} \rightarrow MIL-101(Al):Ru(III)-PEI^{\cdot}+H^{+} \quad (2)$$

$$MIL-101(Al):Ru(III)-PEI^{\cdot} \rightarrow MIL-101(Al):Ru(II)^{*}-PEI \quad (3)$$

$$MIL-101(Al):Ru(II)^{*}-PEI \rightarrow MIL-101(Al):Ru(II)-PEI+h\nu \quad (4)$$

Meanwhile, the quenching efficiency of quenching probe made a powerful influence on the sensitivity of immunosensors. To study the quenching effect of Fe_3O_4@PDA-Cu_xO, two kinds of Ab_2 bioconjugates, Fe_3O_4@PDA-Ab_2 and Fe_3O_4@PDA-Cu_xO-Ab_2, were synthesized. As is depicted in Fig. 3C, ECL response of the immunosensor before modification with Ab_2 bioconjugates was 8968 a. u. (curve a). When Fe_3O_4@PDA-Ab_2 was introduced on the electrode, a distinct decrease in ECL emission was observed (curve b) due to the fact that catechol or benzoquinone units in PDA could quench the excited state of MIL-101(Al):Ru-PEI-Au by means of energy transfer (Liu et al., 2017; Xue et al., 2009). When Fe_3O_4@PDA-Cu_xO-Ab_2 was modified on the electrode, a weak ECL signal about 3862 a. u. in curve c was obtained for the reason that Cu^{2+} adsorbed by the PDA shell could inhibit the excited state MIL-101(Al):Ru (II)* emission via electron transfer (Myers et al., 2009). To get further insight into the quenching ability of Fe_3O_4@PDA-Cu_xO, the fluorescence spectra of MIL-101(Al):Ru and its mixtures were recorded and the results were presented in Fig. 3D. The maximum fluorescence peak of MIL-101(Al):Ru was centered at 622 nm with a fluorescence intensity of 190 a. u. (curve a). While after mixing with Fe_3O_4@PDA and Fe_3O_4@PDA-Cu_xO, MIL-101(Al):Ru experienced a continuous decline in fluorescence intensity (curve b and c), indicating that Fe_3O_4@PDA-Cu_xO was able to inhibit the fluorescence

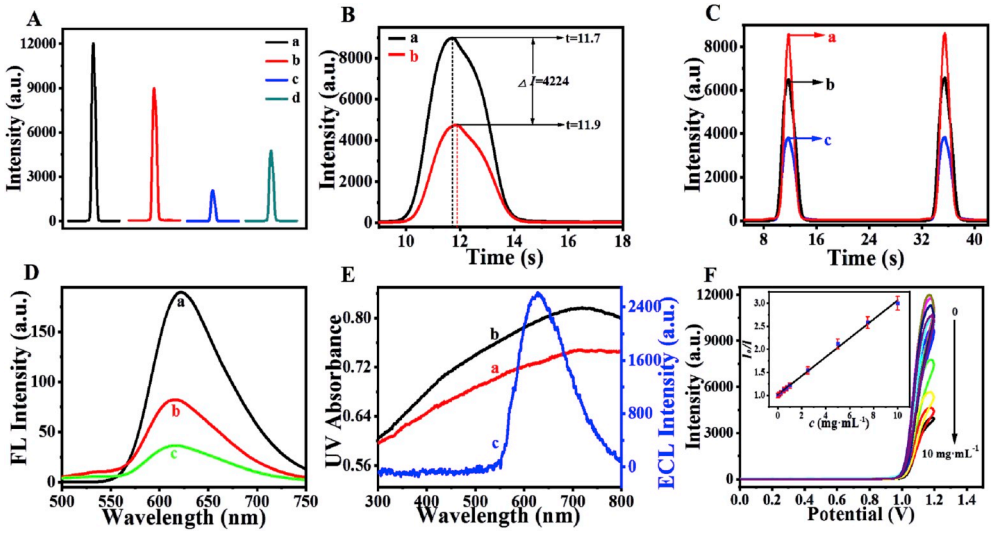

Fig. 3. (A) ECL intensity comparison of (a) MIL-101(Al):Ru-PEI-Au/GCE and (b) MIL-101(Al):Ru-PEI/GCE in 10 mL of PBS (pH 7.4), (c) MIL-101(Al):Ru/GCE in 10 mL of PBS (pH 7.4) containing 10 μL of TPrA, (d) MIL-101(Al):Ru/GCE in 10 mL of PBS (pH 7.4) containing 10 μL of PEI. (B) ECL dynamic curves of (a) MIL-101(Al):Ru-PEI/GCE in 10 mL of PBS (pH 7.4), (b) MIL-101(Al):Ru/GCE in 10 mL of PBS (pH 7.4) containing 10 μL of PEI. (C) quenching effect comparison of different Ab_2 bioconjugates: (a) Ag/BSA/Ab_1/MIL-101(Al):Ru-PEI-Au/GCE, (b) Fe_3O_4@PDA-Ab_2/Ag/BSA/Ab_1/MIL-101(Al):Ru-PEI-Au/GCE, (c) Fe_3O_4@PDA-CuxO-Ab_2/Ag/BSA/Ab_1/MIL-101(Al):Ru-PEI-Au/GCE. (D) fluorescence spectra of (a) MIL-101(Al):Ru, (b) a mixture of MIL-101(Al):Ru and Fe_3O_4@PDA, (c) a mixture of MIL-101(Al):Ru and Fe_3O_4@PDA-Cu_xO. (E) UV–vis spectra of (a) Fe_3O_4@PDA, (b) Fe_3O_4@PDA-Cu_xO and (c) ECL spectra of MIL-101(Al):Ru. (F) ECL intensities of MIL-101(Al):Ru-PEI-Au in the presence of 0, 0.1, 0.25, 0.5, 0.75, 1, 2.5, 5, 7.5, 10 mg mL^{-1} of Fe_3O_4@PDA-Cu_xO. Inset: Stern-Volmer quenching intensity plot of MIL-101(Al):Ru-PEI-Au by Fe_3O_4@PDA-Cu_xO in 10 mL of PBS (pH 7.4).

emission of MIL-101(Al):Ru. What's more, the UV–vis absorption spectra of Fe_3O_4@PDA and Fe_3O_4@PDA-Cu_xO as well as the ECL emission spectra of MIL-101(Al):Ru were also studied. From curve c in Fig. 3E, it could be observed that the ECL spectra of MIL-101(Al):Ru exhibited a maximum emission at around 630 nm. Meanwhile, in contrast to the UV–vis spectra of Fe_3O_4@PDA (curve a), a broader UV–vis absorption range was acquired from Fe_3O_4@PDA-Cu_xO (curve b). The UV–vis absorption spectra of Fe_3O_4@PDA-Cu_xO displayed a noticeable overlap with the ECL emission spectra of MIL-101(Al):Ru, ensuring the occurrence of resonance energy transfer (RET) between the energy donor of Ru@MIL-101 and the energy acceptor of Fe_3O_4@PDA-Cu_xO. The possible quenching mechanisms of Fe_3O_4@PDA-Cu_xO were illustrated as follows.

MIL-101(Al):Ru(II)*-PEI+  → MIL-101(Al):Ru(III)-PEI+  (5)

MIL-101(Al):Ru(II)*-PEI+Cu(II) → MIL-101(Al):Ru(III)-PEI+Cu(I) (6)

It has been well-documented that the quenching effect of quencher could be assessed by quenching rate constant (k_q) according to Stern-Volmer equation (Cao et al., 2006; Xia et al., 1995): $I_0/I = 1 + k_q\tau_0$ [Q] = 1 + K_{sv} [Q]. In this equation, I is the emission intensity in the presence of quencher, I_0 is the emission intensity in the absence of quencher, K_{sv} is the Stern-Volmer constant, k_q is the quenching rate constant, τ_0 is the photoluminescence lifetime, which is 589 ns for Ru $(bpy)_3^{2+}$ in the absence of quencher, [Q] is the quencher concentration. The ECL quenching evaluation of MIL-101(Al):Ru-PEI-Au/GCE by Fe_3O_4@PDA-Cu_xO was conducted in 10 mL of PBS (pH 7.4) containing various concentrations of Fe_3O_4@PDA-Cu_xO (0, 0.1, 0.25, 0.5, 0.75, 1, 2.5, 5, 7.5, 10 mg mL^{-1}), and the results were shown in the inset of Fig. 3F. The plot of I_0/I verses the concentration of Fe_3O_4@PDA-Cu_xO displayed a curve with the slope of 0.20482, thus K_{sv} value of 0.20482 L g^{-1} and k_q value of 3.5 × 10^5 L g^{-1}·s^{-1} were calculated. The high value of quenching rate constant manifested the efficacious quenching ability of Fe_3O_4@PDA-Cu_xO, which providing an efficient strategy to construct signal-quenched type ECL immunosensors.

3.3. Optimization experimental conditions

For purpose of achieving ultrasensitive determination of PCT, the effects of experimental conditions such as the molar ratio of Ru $(bpy)_3^{2+}$ to NH_2-BDC, the amount of $CuCl_2$, the incubation time of Ab_2 bioconjugates and pH of PBS on the ECL intensity were evaluated. The molar ratio of Ru $(bpy)_3^{2+}$ to NH_2-BDC during the preparation of MIL-101(Al):Ru played a pivotal role in the initial ECL intensity of "signal-on" state. MIL-101(Al):Ru with different molar ratios of Ru $(bpy)_3^{2+}$ to NH_2-BDC (1:2, 1:4, 1:6, 1:8) were denoted as MIL-101(Al):Ru (2), (4), (6), (8) respectively. Observed from Fig. 4A, on the one hand, though the ECL intensities of MIL-101(Al):Ru (2) and MIL-101(Al):Ru (4) were stronger than that of MIL-101(Al):Ru (6), their ECL stabilities were undesirable because both MIL-101(Al):Ru (2) and MIL-101(Al):Ru (4) were made up of abundant Ru $(bpy)_3^{2+}$ with good water-solubility. On the other hand, in spite of the approving ECL stability of MIL-101(Al):Ru (10), the ECL response of MIL-101(Al):Ru (6) was far beyond that of MIL-101(Al):Ru (8) and MIL-101(Al):Ru (10). Therefore, the molar ratio of Ru $(bpy)_3^{2+}$ to NH_2-BDC was chosen as 1:6 to synthesize MIL-101(Al):Ru with strong ECL intensity and satisfying stability. Meanwhile, to achieve the high-efficiency quenching of luminophore, the concentration of $CuCl_2$ was optimized and the result was displayed in Fig. 4B. The ECL intensity descended dramatically with the concentration of $CuCl_2$ rising from 5 mM to 20 mM, while it turned to be stabilized ultimately with further augment of $CuCl_2$ content, which probably due to the adsorption of cupric ion by the PDA surface attained its saturate state. Thereafter, to avoid the waste of reagent and achieve effective quenching effect, 25 mM of $CuCl_2$ was adopted for the preparation of Fe_3O_4@PDA-Cu_xO. The incubation time of immunocomplexes was also optimized as shown in Fig. 4C. The ECL intensity witnessed a sharp drop as the incubation time prolonged from 30 min to 70 min and after that, the ECL intensity arrived its plateau. Accordingly, a suitable incubation time of 70 min was selected in the following experiment. Besides, PBS that covering the pH range from 6.5 to 8.5 was chosen to explore the influence of pH on the ECL intensity. Apparently, pH 7.5 was adopted in the subsequent work for better biological activities of PCT and higher ECL response of the immunosensor.

3.4. Analytical performance of the ECL immunosensor

In this work, PCT with different concentrations were chosen as model analyte to access the analytical performance of the proposed immunosensor under optimum conditions. As is portrayed in Fig. 5A, the ECL intensity descended as the PCT concentration increased continuously. A plot of ECL intensity versus the logarithm of PCT concentration in Fig. 5B was linear from 0.0005 ng mL^{-1} to 100 ng mL^{-1}, and the curve was well fitted with the following equation:

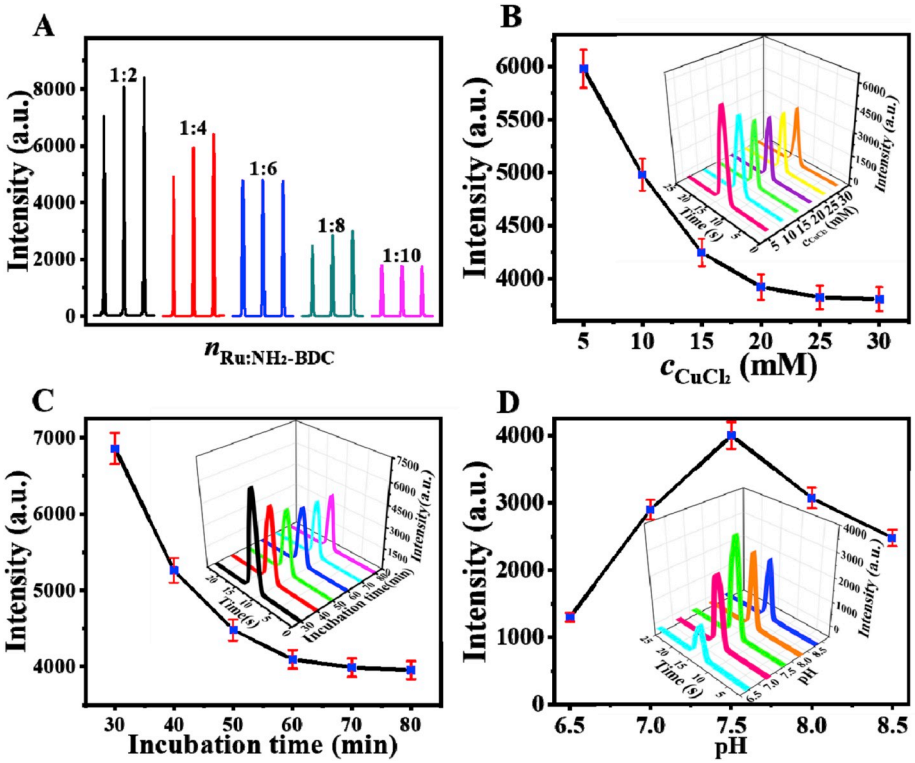

Fig. 4. Optimization of (A) molar ratio of Ru $(bpy)_3^{2+}$ to NH_2-BDC, (B) concentration of $CuCl_2$, (C) incubation time of Ab_2 bioconjugates, (D) pH value of PBS.

I = 4292.5–1845.5 lg c (where I is the ECL intensity and c represents the concentration of PCT, ng·mL^{-1}). The square of correlation coefficient (R^2) was 0.9938, and the limit of detection (LOD) was figured to be 0.18 pg mL^{-1} according to the definition of LOD prescribed by IUPAC(Long and Winefordner, 1983). In comparison with the analytical performances of other PCT immunosensors, the proposed strategy was comparable or even better to the literatures listed in Table S2 owing to the remarkable ECL property of MIL-101(Al):Ru-PEI-Au and highly-efficient quenching ability of Fe_3O_4@PDA-Cu_xO.

3.5. Application in human serum

To evaluate the clinical application prospect of this PCT immunoassay, recovery experiments were implemented in human serum samples by standard addition method. Two kinds of human serum samples were obtained from healthy individual and people who suffered from inflammation, respectively. Firstly, PCT contents of these 5-fold-diluted serum samples were tested five times parallelly, thus average value of 0.018 ng mL^{-1} and 23.7 ng mL^{-1} were figured, respectively. Then, appropriate amounts of PCT standard solution (denoted as Added) were spiked into corresponding samples and the corresponding PCT concentrations of these samples were obtained (denoted as Found) after the ECL response measured for five times. As illustrated in Table S3, the RSD was calculated to be within 8% with acceptable recoveries varied from 94% to 101.6%. Moreover, we challenged the accuracy and precision of our ECL immunoassay with

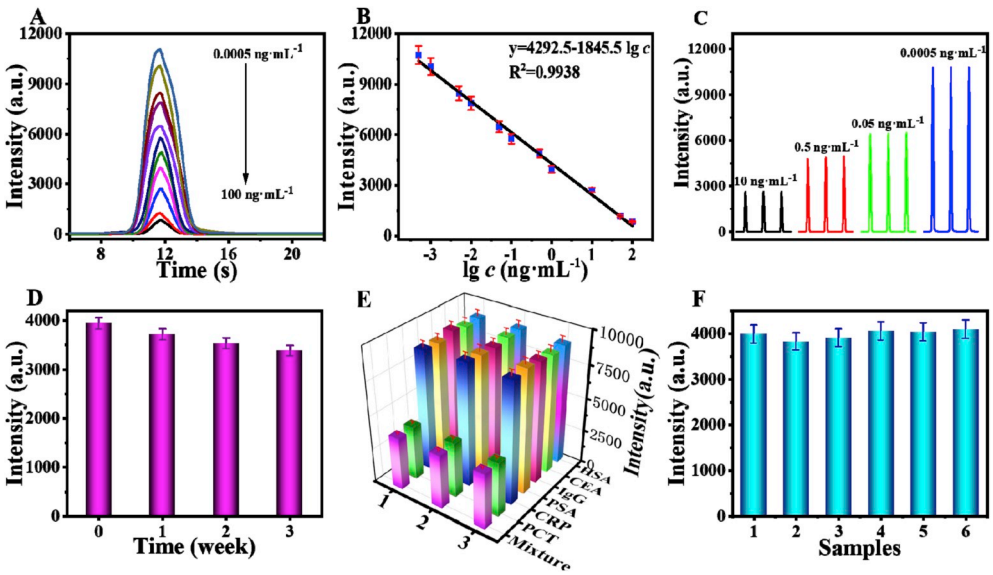

Fig. 5. (A) ECL intensity-time curves of the immunosensor in the presence of different concentrations of PCT: 0.0005, 0.001, 0.005, 0.01, 0.05, 0.1, 0.5, 1, 10, 50, 100 ng mL^{-1}. (B) Calibration plots of the immunosensor. (C) stability of the immunosensor to various concentrations of PCT. (D) Long-term storage stability of the sensor incubated with 1 ng mL^{-1} of PCT. (E) Selectivity of the immunosensor: 10 ng mL^{-1} of HSA, CEA, IgG, PSA, CRP and 1 ng mL^{-1} of PCT with their mixture. (F) Reproducibility of the immunosensor incubated with 1 ng mL^{-1} of PCT.

conventional enzyme-linked immunosorbent assay (ELISA) kit by F-test and *t*-test. The results were exhibited in Table S4, from which it could be observed that the calculated F value was far below the theoretical one (the theoretical F value was 6.39 when the degree of freedom (f) was 4 and the confidence level (P) was 95%), and the *t* value was much less than the theoretical *t* value (t_{theory} = 2.31 when f = 8, P = 95%), elucidating that there was nearly no significant difference between the two methods. Given this, the proposed immunosensor hold immense application potential in clinical detection of PCT.

4. Conclusions

A "signal on-off" type ECL immunosensor is constructed in this study for PCT detection based on double quenching effects of Fe_3O_4@PDA-Cu_xO towards self-enhanced MIL-101(Al):Ru-PEI-Au complexes. Such an ultrasensitive ECL immunosensor present the following attractive aspects. Firstly, the high specific surface area and inherent mesoporous structure of MIL-101(Al)–NH_2 endow it with the ability to load Ru $(bpy)_3^{2+}$ abundantly. The resulted luminescence functionalized MOF couple with PEI as the coreactant form self-enhanced Ru-PEI complexes, and Au NPs are further immobilized on it to obtain a "signal-on" state with strong ECL emission. Besides, Fe_3O_4@PDA-Cu_xO-Ab_2 is employed as the quenching probe to achieve high quenching efficiency for the reason that catechol or benzoquinone units in PDA and Cu^{2+} adsorbed by PDA could quench the excited states of Ru $(bpy)_3^{2+}$ via electron transfer and resonance energy transfer. The MIL-101(Al):Ru luminophore prepared in this work for the first time might open up an innovative direction to synthesize luminescence-functionalized MOFs, and the proposed ECL immunosensor with desirable stability and selectivity could be a robust and reliable tool in clinical analysis of PCT and other biomarkers.

Declaration of competing interest

The authors declare that they have no known competing financial interests or personal relationships that could have appeared to influence the work reported in this paper.

CRediT authorship contribution statement

Chao Wang: Conceptualization, Data curation, Writing - original draft. **Nuo Zhang:** Methodology, Writing - review & editing. **Dong Wei:** Methodology. **Rui Feng:** Formal analysis. **Dawei Fan:** Methodology, Writing - review & editing. **Lihua Hu:** Formal analysis. **Qin Wei:** Funding acquisition, Project administration. **Huangxian Ju:** Formal analysis.

Acknowledgements

This study was supported by the National Key Scientific Instrument and Equipment Development Project of China (No.21627809), National Natural Science Foundation of China (Nos. 21505051, 21575050, 21607055, 21777056), Jinan Scientific Research Leader Workshop Project (2018GXRC024).

Appendix A. Supplementary data

Supplementary data to this article can be found online at https://doi.org/10.1016/j.bios.2019.111521.

References

Baldini, F., Bolzoni, L., Giannetti, A., Kess, M., Kramer, P.M., Kremmer, E., Porro, G., Senesi, F., Trono, C., 2009. Anal. Bioanal. Chem. 393, 1183–1190.
Cao, W., Ferrance, J.P., Demas, J., Landers, J.P., 2006. J. Am. Chem. Soc. 128, 7572–7578.
Chen, A., Zhao, M., Zhuo, Y., Chai, Y., Yuan, R., 2017. Anal. Chem. 89, 9232–9238.
Cui, Y., Yue, Y., Qian, G., Chen, B., 2012. Chem. Rev. 112, 1126–1162.
Du, F.K., Zhang, H., Tan, X.C., Yan, J., Liu, M., Chen, X., Wu, Y.Y., Feng, D.F., Chen, Q.Y., Cen, J.M., Liu, S.G., Qiu, Y.Q., Han, H.Y., 2018. Biosens. Bioelectron. 106, 50–56.
El Haddad, H., Chaftari, A.M., Hachem, R., Chaftari, P., Raad II, , 2018. Clin. Infect. Dis. 67, 971–977.
Fang, Y., Hu, Q., Yu, X., Wang, L., 2018. Sens. Actuators B Chem. 258, 238–245.
Hao, N., Xiong, M., Zhang, J.D., Xu, J.J., Chen, H.Y., 2013. Anal. Chem. 85, 11715–11719.
Haque, E., Lo, V., Minett, A.I., Harris, A.T., Church, T.L., 2014. J. Mater. Chem. 2, 193–203.
Hong, L.R., Chai, Y.Q., Zhao, M., Liao, N., Yuan, R., Zhuo, Y., 2015. Biosens. Bioelectron. 63, 392–398.
Hu, W., He, G., Zhang, H., Wu, X., Li, J., Zhao, Z., Qiao, Y., Lu, Z., Liu, Y., Li, C.M., 2014. Anal. Chem. 86, 4488–4493.
Lee, H., M Dellatore, S., Miller, W., B Messersmith, P., 2007. Sci 318 (5849), 426–430.
Lei, Y.M., Zhao, M., Wang, A., Yu, Y.Q., Chai, Y.Q., Yuan, R., Zhuo, Y., 2016. Chem. Eur J. 22, 8207–8214.
Li, L., Chen, Y., Zhu, J.J., 2017a. Anal. Chem. 89, 358–371.
Li, X., Wang, Y., Shi, L., Ma, H., Zhang, Y., Du, B., Wu, D., Wei, Q., 2017b. Biosens. Bioelectron. 96, 113–120.
Li, Y., Liu, W., Jin, G., Niu, Y., Chen, Y., Xie, M., 2018. Anal. Chem. 90, 8002–8010.
Liao, N., Zhuo, Y., Chai, Y., Xiang, Y., Cao, Y., Yuan, R., Han, J., 2012. Chem. Commun. 48, 7610–7612.
Liao, N., Zhuo, Y., Chai, Y.Q., Xiang, Y., Han, J., Yuan, R., 2013. Biosens. Bioelectron. 45, 189–194.
Liu, Y., Zhao, Y., Zhu, Z., Xing, Z., Ma, H., Wei, Q., 2017. Anal. Chim. Acta 963, 17–23.
Long, G.L., Winefordner, J.D., 1983. Anal. Chem. 55, 712–724.
Mei, Y.L., Wang, H.S., Li, Y.F., Pan, Z.Y., Jia, W.L., 2010. Electroanalysis 22, 155–160.
Myers, C.P., Miller, J.R., Williams, M.E., 2009. J. Am. Chem. Soc. 131, 15291–15300.
Qin, X., Zhang, X., Wang, M., Dong, Y., Liu, J., Zhu, Z., Li, M., Yang, D., Shao, Y., 2018. Anal. Chem. 90, 11622–11628.
Sener, G., Ozgur, E., Rad, A.Y., Uzun, L., Say, R., Denizli, A., 2013. Analyst 138, 6422–6428.
Tokel, N.E., Bard, A.J., 1972. J. Am. Chem. Soc. 94, 2862–2863.
Vincenzi, B., Fioroni, I., Pantano, F., Angeletti, S., Dicuonzo, G., Zoccoli, A., Santini, D., Tonini, G., 2016. Sci. Rep. 6, 28090–28095.
Wang, H., Peng, L., Chai, Y., Yuan, R., 2017. Anal. Chem. 89, 11076–11082.
Wang, H., Yuan, Y., Chai, Y., Yuan, R., 2015. Biosens. Bioelectron. 68, 72–77.
Wang, J.X., Zhuo, Y., Zhou, Y., Wang, H.J., Yuan, R., Chai, Y.Q., 2016a. ACS Appl. Mater. Interfaces 8, 12968–12975.
Wang, Y.Z., Hao, N., Feng, Q.M., Shi, H.W., Xu, J.J., Chen, H.Y., 2016b. Biosens. Bioelectron. 77, 76–82.
Xia, X.B., Ding, Z.F., Liu, J.Z., 1995. J. Photochem. Photobiol. A Chem. 88, 81–84.
Xiong, C., Liang, W., Zheng, Y., Zhuo, Y., Chai, Y., Yuan, R., 2017. Anal. Chem. 89, 3222–3227.
Xue, L., Guo, L., Qiu, B., Lin, Z., Chen, G., 2009. Electrochem. Commun. 11, 1579–1582.
Yang, M., Chen, Y., Xiang, Y., Yuan, R., Chai, Y., 2013. Biosens. Bioelectron. 50, 393–398.
Yue, X., Zhu, Z., Zhang, M., Ye, Z., 2015. Anal. Chem. 87, 1839–1845.
Zhang, C.Y., Gao, J., Wang, Z., 2018. Adv. Mater. 30, 1803618–1803627.
Zhang, S., Zhang, Y., Bi, G., Liu, J., Wang, Z., Xu, Q., Xu, H., Li, X., 2014. J. Hazard Mater. 270, 27–34.
Zhao, M., Chen, A.Y., Huang, D., Zhuo, Y., Chai, Y.Q., Yuan, R., 2016. Anal. Chem. 88, 11527–11532.
Zhao, M., Liao, N., Zhuo, Y., Chai, Y.Q., Wang, J.P., Yuan, R., 2015. Anal. Chem. 87, 7602–7609.
Zhou, Y., Chen, S., Luo, X., Chai, Y., Yuan, R., 2018. Anal. Chem. 90, 10024–10030.
Zhu, Q.L., Xu, Q., 2014. Chem. Soc. Rev. 43, 5468–5512.
Zhuo, Y., Liao, N., Chai, Y.Q., Gui, G.F., Zhao, M., Han, J., Xiang, Y., Yuan, R., 2014. Anal. Chem. 86, 1053–1060.